The Cryosphere Discuss., 9, 6829–6870, 2015
www.the-cryosphere-discuss.net/9/6829/2015/
doi:10.5194/tcd-9-6829-2015

The Cryosphere Discussions
Open Access
EGU

On the assimilation of optical reflectances and snow depth observations into a detailed snowpack model

L. Charrois[1,2], E. Cosme[1], M. Dumont[2], M. Lafaysse[2], S. Morin[2], Q. Libois[1], and G. Picard[1]

[1]Université Grenoble Alpes-CNRS, LGGE, UMR 5183, Grenoble, France
[2]Météo-France/CNRS, CNRM-GAME UMR 3589, CEN, St. Martin d'Hères, France

Received: 20 October 2015 – Accepted: 25 November 2015 – Published: 14 December 2015

Correspondence to: L. Charrois (luc.charrois@gmail.com)

Published by Copernicus Publications on behalf of the European Geosciences Union.

Abstract

This paper examines the ability of optical reflectance data assimilation to improve snow depth and snow water equivalent simulations from a detailed multilayer snowpack model. The direct use of reflectance data, instead of higher level snow products, rules out uncertainties due to commonly used retrieval algorithms. Data assimilation is performed with an ensemble-based method, the Sequential Importance Resampling Particle filter, to represent simulation uncertainties. Here, model uncertainties are essentially ascribed to meteorological forcings. An original method of stochastic perturbation is implemented to explicitly simulate the consequences of these uncertainties on the snowpack estimates.

The assimilation of spectral reflectances from the MODerate Imaging Spectrometer (MODIS) sensor is examined, through twin experiments based on synthetic observations, over five seasons at the Col du Lautaret, located in the French Alps. Overall, the assimilation of MODIS-like data reduces root mean square errors (RMSE) on snow depth and snow water equivalent by a factor of 2. At this study site, the lack of MODIS data on cloudy days does not affect the assimilation performance significantly. The combined assimilation of MODIS-like reflectances and a few snow depth measurements throughout the 2010/11 season further reduces RMSEs by a factor of roughly 3.5. This work suggests that the assimilation of optical reflectances should become an essential component of spatialized snowpack simulation and forecast systems. The assimilation of real MODIS data will be investigated in future works.

1 Introduction

Seasonal snowpack modeling is a crucial issue for a large range of applications, including the forecast of natural hazards such as avalanches or floods, or the study of climate change (e.g. Durand et al., 1999; Lehning et al., 2006; Bavay et al.,

TCD
9, 6829–6870, 2015

2013). The most sophisticated detailed snowpack models represent the evolution of snow microstructure and the layering of snow physical properties (Brun et al., 1989, 1992; Jordan, 1991; Bartelt and Lehning, 2002; Vionnet et al., 2012) in response to meteorological conditions. Despite constant efforts to improve these models, large uncertainties remain in the representation of the snow physics, as well as in the meteorological forcings (Carpenter and Georgakakos, 2004; Essery et al., 2013; Raleigh et al., 2015). These uncertainties are highly amplified when propagated to avalanche hazard models (Vernay et al., 2015). For operational applications, the assimilation of observations can help reducing the impact of the model and forcing uncertainties in the snowpack simulations (e.g. Dechant and Moradkhani, 2011) using microwave radiance data.

In situ measurements are the most detailed and accurate observations of the snowpack, but their spatial distribution is far too scarce to capture the high spatial variability of the snowpack properties. Satellite observations are much more appropriate for this purpose. Their main limitation is to provide a surface-only or a vertically integrated information on the snowpack, which is not always straightforward to connect to the snow properties. This obstacle can be circumvented using satellite-based snow products such as Snow Water Equivalent (SWE) estimates from passive microwave sensors (Andreadis and Lettenmaier, 2006; Dong et al., 2007; De Lannoy et al., 2012), snow cover fraction (Liu et al., 2013) or albedo (Dumont et al., 2012) from optical sensors. However, satellite snow products are derived using retrieval algorithms which are not perfect and, perhaps more importantly, not physically consistent with the snowpack model used for the data assimilation. For this reason, and as advocated by Durand et al. (2009), assimilating the original satellite radiance data should be preferred when possible.

Snow remote sensing is primarily performed in the microwave (passive and active), visible and near-infrared spectra. The potential of assimilating passive microwave radiances collected by AMSR-E satellite have been examined by e.g. Dechant and Moradkhani (2011) in the context of streamflow forecasting. But the coarse

TCD
9, 6829–6870, 2015

spatial resolution of these data considerably reduces their usefulness for small-scale applications in mountainous areas (Foster et al., 2005; Cordisco et al., 2006; Dong et al., 2007; Tedesco et al., 2010). As for active microwave, several tests have been conducted to assimilate the satellite signal (e.g. Stankov et al., 2008; Phan et al., 2014). These tests were however limited by the accuracy of the forward electromagnetic models and by the current lack of satellite data at a daily or even weekly time frequency.

Visible and near-infrared reflectances from satellite observations have never been assimilated into snowpack models despite their great sensitivity to the snowpack properties (Warren, 1982). Even if cloud cover might limit their utility, medium and high spatial resolution data are available at daily resolution from several optical sensors (e.g. MODerate Imaging Spectrometer, Visible Infrared Imaging Radiometer Suite) and seem to be quite suitable for complex topography (Sirguey et al., 2009). In particular, the MODIS sensor, on board TERRA and AQUA satellites, offers a daily coverage and provides reflectance measurements in seven bands distributed in the visible (at 250 to 500 m spatial resolution), near and short-wave infrared wavelengths. Surface bi-hemispherical reflectances corrected from complex topographic effects in mountainous areas can be computed (Sirguey et al., 2009) and have been evaluated and used in several rugged areas (Dumont et al., 2012; Brun et al., 2015).

The work presented in this article examines the possibility, the relevance and the limitations of assimilating visible and near-infrared satellite reflectances into a multilayer snowpack model. Only synthetic observations (simulated by the assimilative model) are used in this work, to examine the content of information of the observations, and the impacts we can expect from their assimilation. Data assimilation is performed with a particle filter and a Sequential Importance Resampling (SIR) algorithm (Gordon et al., 1993; Van Leeuwen, 2009, 2014). The particle filter is easy to implement, free of hypotheses about the nature of the model and the observations, and provides uncertainties in the estimation of the snowpack state.

For a comprehensive snow simulations evaluation, as recommended by Essery et al. (2013), our study is based on 5 hydrological seasons (2005/06, 2006/07, 2009/10,

TCD
9, 6829–6870, 2015

2010/11, 2011/12) which represent a wide range of possible snow cover conditions in the Alpine area. Moreover, 2 experimental sites were used in this work in virtue of a long, continuous time serie of meteorological data and an area suitable to remote sensing measurements. Indeed, the Col de Porte (CdP) area, located in the Chartreuse area, near Grenoble, France (1325 m a.s.l.) provides a data set from 1993 to present (Morin et al., 2012) from which meteorological statistic can be estimated, but the instrumentation and surrounding forest at this site may affect satellite measurements. For this reason, assimilation experiments are carried out at the Col du Lautaret (CdL) located (2058 m a.s.l.) in the Ecrins area, France, which exhibits a large flat open area, above treeline, more suitable for remote sensing.

In Sect. 2, the SURFEX/ISBA – Crocus snowpack model used in this study is described with an emphasis on the characteristics that affect the implementation of the data assimilation method. In particular, we consider the meteorological forcings as the only source of uncertainties. Section 3 presents in details how these forcings are perturbed to take the uncertainties into account in the design of the ensemble simulations. The experimental setup and the data assimilation implementation are presented in Sect. 4. The results of the reference assimilation experiment (baseline experiment) using reflectance observations at one point are presented and discussed in Sect. 5. In close relation to this previous experiment, results of different sensitivity tests are addressed in Sect. 6.

2 SURFEX/ISBA – Crocus

2.1 A brief overview

The unidimensional detailed multilayer snowpack model Crocus (Brun et al., 1989, 1992) simulates the evolution of the snowpack physical and microstructural properties driven by near-surface meteorology and including a representation of snow metamorphism. A detailed description of Crocus is provided by Vionnet et al. (2012);

TCD
9, 6829–6870, 2015

here we only emphasize aspects that are key to data assimilation. The snowpack is vertically discretized into snow layers with different physical properties and a dynamical layering scheme handles its evolution (see details in Sect. 2.2). The evolution of the snow cover is a function of energy and mass transfer between the snowpack and the atmosphere and the ground. The model simulates the major physical processes of snowpack evolution such as heat conduction, light penetration, water percolation and refreezing, settlement and snow metamorphism.

Crocus has been run operationally at Météo-France in support of the avalanche risk forecasting over the last 20 years (Durand et al., 1999). It has been also successfully used for various applications such as climate studies or hydrology (e.g. Etchevers et al., 2001; Castebrunet et al., 2014). Recently, Crocus has been integrated into the SURFEX externalized surface modeling system (Masson et al., 2013) as one of the snow schemes within the Interactions between Soil, Biosphere and Atmosphere (ISBA) land surface model (Noilhan and Planton, 1989). Thus the integrated system simulates the energy fluxes between the snow cover and the multilayer soil component of the land surface model (ISBA-DIF, Boone and Etchevers, 2001).

2.2 Layering

In Crocus, the snowpack is vertically discretized in order to realistically simulate the time evolution of a stratified snowpack. The layering scheme is dynamical so as to preserve snowpack history and maintain the possible thin and weak snow layers within the snowpack. The number of layers ranges from 0 (bare soil) to a maximum of 50, typically. Layering is updated at the beginning of each time step. It consists in adding, removing, or merging layers depending on their physical properties and thicknesses. The procedure basically follows this set of rules:

- For a snowfall on an existing snowpack, fresh snow is incorporated into the top layer if snow microstructure characteristics are similar and if the amount of new snow is below a prescribed threshold. Otherwise, a new layer is created.

TCD
9, 6829–6870, 2015

- A snowfall on bare soil forms a snowpack with identical layers, the number of which depends on the quantity of fallen snow.
- In absence of snowfall, the model seeks first to merge two thin and adjacent layers with similar microstructure characteristics, or inversely, split the thick ones. When the number of layers has reached its maximum of 50, layer that is too small relatively to a prescribed optimal vertical profile is aggregated with an adjacent one.
- Most of the time, compaction makes layers thinner without grid resizing.

Dynamical layering adds an extra challenge in the assimilation of observations with Crocus. Data assimilation methods commonly used in geophysics are well designed for fixed-grid models. For example, the Ensemble Kalman filter involves the averaging of different snow profiles. This specificity of Crocus largely determines our data assimilation method, as it will be discussed in Sect. 4.3.

2.3 Penetration of solar light in the snowpack

A new radiative transfer model, recently implemented in Crocus, provides spectral reflectances that can be used for the comparison and the assimilation of satellite data such as MODIS. This model, named TARTES (Two-streAm Radiative TransfEr in Snow, Libois et al., 2013, 2014), simulates the absorption of solar radiation within the stratified snowpack using the δ-Eddington approximation, with a spectral resolution of 10 nm. This contrasts with the original version of Crocus, where albedo was computed for three large spectral bands only and from the properties of the first two layers (Brun et al., 1992; Vionnet et al., 2012). The radiative transfer is driven by the physical properties of the snowpack (specific surface area, density, snow layer thickness, impurity content and shape parameters) and the angular and spectral characteristics of the incident radiance (e.g. the solar zenith angle and the presence of cloud cover). In particular,

TCD
9, 6829–6870, 2015

impurities affect the absorption coefficient and the concentration of impurities can be prescribed in the radiative scheme.

2.4 Snow impurities

Snow surface reflectance in the visible spectrum depends on the content of light-absorbing impurities in the snowpack (Warren, 1982). The impurity content can have a major impact on the snowpack simulations (Dumont et al., 2014). Despite efforts to improve the knowledge and the modeling of impurities in snow (e.g. Warren and Clarke, 1990; Domine et al., 2004; Painter et al., 2007; Doherty et al., 2013), snow impurity deposition and evolution remain poorly quantified.

Currently implemented in a version of SURFEX/ISBA – Crocus, the radiative model TARTES (introduced in Sect. 2.3) calculates the impurity content as an equivalent black carbon content (Doherty et al., 2013; Gabbi et al., 2015). This impurity content evolves according to (i) the impurity content in fresh snow, c_0, (ii) the time of exposure of the layer at the surface and (iii) the dry deposition flux of impurity, τ_{dry} as described in the equation below.

$$c(t + \Delta t) = c(t) + \Delta t\, \tau_{\mathrm{dry}} \mathrm{e}^{-D/h_{\mathrm{ref}}} \quad (1)$$

where $c(t)$ is the impurity content at time t, D is the depth of the middle of the considered snow layer and $h_{\mathrm{ref}} = 5\,\mathrm{cm}$ is the e-folding of the exponential decay rate for the deposition of snow impurities ensuring that only the top layers are influenced by dry deposition.

2.5 Atmospheric forcings

The snowpack evolution strongly depends on near-surface meteorological forcings. These forcings are provided by the meteorological downscaling and analysis tool SAFRAN (Durand et al., 1993). SAFRAN is used to drive snowpack simulations in the French mountains because it is designed to operate at the geographical

TCD
9, 6829–6870, 2015

scale of meteorologically homogeneous mountain ranges. This model provides input meteorological data to the snowpack model with an hourly time step for all slopes and aspects, with 300 m elevation step. The forcing variables are air temperature, specific humidity, wind speed, precipitation amount and phase, direct and diffuse solar radiation and longwave downward flux (Durand et al., 1993).

3 Design of Crocus ensemble simulations

3.1 General strategy

In view of assimilating observations to reduce snowpack simulation uncertainties, we first need to actually simulate the errors affecting the snowpack simulation. As shown in Raleigh et al. (2015), the meteorological forcings are the major source of uncertainty in snowpack simulations when a meteorological model is used to drive the snow model. In the present study, air temperature, wind speed, snowfall and rainfall rates, shortwave and longwave radiative fluxes, and the deposition rate of impurities will thus be considered as the only sources of uncertainty. Snowpack model errors introduced by metamorphism and other physical laws parametrization are not taken into account in this study.

We implement an ensemble method to represent the uncertainties in the forcings and their impact on snowpack simulations. An ensemble of possible realizations of the atmospheric forcings is formed and used to compute an ensemble of snow profiles representing the probability distribution of the model simulation. The present section describes the construction of the ensemble of meteorological forcings and the response of the model to this source of uncertainty, without assimilation.

3.2 Quantification of meteorological forcing uncertainties

To quantify and calibrate the meteorological forcing uncertainties, we compare 18 years of surface meteorology from SAFRAN reanalysis with in situ observations at the CdP.

TCD
9, 6829–6870, 2015

A long time-series from 1993 to present (Morin et al., 2012) being available at this site, uncertainties in the SAFRAN meteorological reanalysis can be estimated.

Table 1 (left column) reports the bias and the standard deviation of the difference between SAFRAN and the observations carried out at the CdP site, for each meteorological variable (the right column reports other data discussed later). The table reflects significant differences between SAFRAN and in situ observations, resulting from the different spatial representativities of both sources and from the intrinsic errors of the analysis system.

As highlighted by Quintana Segui et al. (2008) who conducted an extended evaluation of SAFRAN reanalysis but over a shorter period (one year), the large discrepancies between the model and the observations can be explained by local effects due to orography and vegetation and, for the precipitation and wind speed, by the hourly interpolation from the daily analysis. Durand et al. (2009) carried out, only on a limited set of variables, a more systematic evaluation of SAFRAN for the 1958–2002 period using 43 sites in the French Alps. Their results are similar in terms of Root Mean Square Error on the air temperature bus this study also highlights the spatial variability of SAFRAN performance.

3.3 Building the ensemble of meteorological forcings

The sample of meteorological forcings is formed by perturbing the original SAFRAN reanalysis with a random noise commensurate with the actual uncertainty. We thus build an ensemble of meteorological forcings with a null bias with regard to the SAFRAN reanalysis and a standard deviation close to the one computed from CdP statistics (Table 1, left column).

To keep the procedure simple and preserve physically consistent time variations of the forcings, the random perturbations are computed using a First Order AutoRegressive (AR(1)) model (Deodatis and Shinozuka, 1988) for each variable:

$$X_t = \varphi X_{t-1} + \epsilon_t, \quad (2)$$

TCD
9, 6829–6870, 2015

with X being the perturbation value at time t and $t-1$. φ is the AR(1) model parameter and can be written $\varphi = e^{\frac{-\Delta t}{\tau}}$, Δt being the time step and τ the decorrelation time. The meteorological uncertainties are introduced with ε_t, a white noise process with zero mean and constant variance σ^2 computed from each standard deviation (Table 1, left column).

For each meteorological variable, the selection of an additive or multiplicative perturbation method is driven by (i) the nature of the variable, and (ii) the dependency of the model-measurement difference to the measured values. Perturbations are thus considered additive for air temperature, wind speed, shortwave flux, and multiplicative for precipitation rates and longwave radiations. For the multiplicative method, the perturbations are bounded to avoid too large values. The result from this perturbation method is illustrated by Fig. S1 in the Supplement which shows the snowfall rates over a week period, as described by SAFRAN reanalysis, a realization of the perturbed analysis, and the full ensemble of perturbed analysis. The decorrelation time, τ, is adjusted for each variable to produce a temporal variation of the perturbed variables similar to the one of the original variables (Fig. S1 bottom, in blue). To maintain physical consistency between the meteorological variables, snowfall is changed to rainfall if air temperature is higher than 274.5 K and the shortwave radiation is bounded to 200 $\mathrm{W\,m^{-2}}$ in case of rain or snow fall.

Moreover, the choice of a multiplicative method for precipitation is motivated by the fact that SAFRAN reanalysis capture well the occurrence of precipitation (because it uses surface observation network) but are more subject to errors in the amount of precipitation.

Ensembles are generated with model errors coming from the statistics of the CdP site but as explained previously, the assimilation framework is based on the CdL area. Some adjustments in the building of ensembles are also required to take into account differences between these 2 areas. In particular the forest is masking part of the shortwave radiation modifying the longwave flux at the CdP site and the local wind field which explains the large discrepancies between the model and the observations.

TCD
9, 6829–6870, 2015

This is not the case for the CdL which is an open meadow area. For these reasons, and after some sensitivity tests focused on shortwave and longwave radiations, the standard deviation used in the AR(1) equation for short and longwave radiations were reduced to, respectively, 70 and 7 $\mathrm{W\,m^{-2}}$, against 79 and 24.5 $\mathrm{W\,m^{-2}}$ (Table 1). The standard deviation computed from the ensemble (right column) are close to the ones prescribed to generate the ensemble (left column).

In the end, this stochastic method of perturbations makes possible the construction of an ensemble of perturbed forcings which are required when using ensemble methods. The calibration of the perturbations are based on the CdP statistics while their temporal correlation is ensured by the AR(1) model. The perturbation method exhibits some obvious limitations. Inter-variables correlations are indeed not taken into account in the ensemble except from the precipitation phase and the maximum value of shortwave radiation in case of precipitation. But this is not crucial in our twin experiment context. Real data assimilation experiment might require a more physically consistent ensemble, this will be investigated in future work.

3.4 Perturbation of impurity deposition rate

In this study, the deposition fluxes of impurities are also considered as a meteorological forcing but unlike meteorological variables previously mentioned (Sect. 2.5), the deposition fluxes of impurities is not provided by the SAFRAN model. Instead, the impurity content in fresh snow c_0 and their dry deposition flux τ_{dry} are perturbed online during a model run.

The parameters c_0 and τ_{dry} are subject to multiplicative perturbations drawn from lognormal distributions. The perturbations are constant in time, but are reinitialized at each observational update when data assimilation is performed. For c_0, the probability density function (pdf) parameters are $\sigma = 0.8$ and $\mu = 0$. c_0 is bounded at 0 and 500 $\mathrm{ng\,g^{-1}}$ and the mode value of the pdf is 100 $\mathrm{ng\,g^{-1}}$. As for τ_{dry}, the pdf parameters are $\sigma = 1.2$ and $\mu = 0$. τ_{dry} is bounded at 0 and 0.5 $\mathrm{ng\,g^{-1}\,s^{-1}}$ with a mode value

TCD
9, 6829–6870, 2015

of $0.015\,\mathrm{ng\,g^{-1}\,s^{-1}}$. These values have been selected to obtain the same order of magnitude of albedo decrease with snow age as in the original Crocus formulation (Brun et al., 1992).

3.5 Ensemble simulations

To investigate the impact of the stochastic perturbations, an ensemble of 300 simulations of the snowpack, forced by the 300 forcings of the meteorological ensemble, is run over the 2010/11 hydrological season without data assimilation. Figure 1 presents the time evolution of the reflectance at 640 nm (first MODIS band central wavelength), snow depth (SD), and snow water equivalent (SWE), for the ensemble (blue envelops) and for the snowpack model run with unperturbed forcings from SAFRAN reanalysis (red lines). The 300 ensemble members are represented by the black lines. The simulation forced by the unperturbed reanalysis is included within the envelop of the ensemble. The spread of the ensemble reflects the consequences of possible overestimations and underestimations of meteorological data by the reanalysis.

The spread of the SD and SWE ensembles (Fig. 1b and c) is the largest at the end of the season, leading to 24 days spread on the melt-out date. The maximum dispersion range ($\Delta\mathrm{SWE} \approx 300\,\mathrm{kg\,m^{-2}}$) occurs in early April. At this time, some ensemble members have just started to melt, while some others have already disappeared.

Snowfalls reset all members to high reflectance values (at 640 nm, 0.98 for a significant event, Fig. 1a) and drastically reduce the spread of the reflectance ensemble. Concomitantly, the SD and SWE ensemble spreads can increase due to the uncertainties in the precipitation rates. After a snowfall, impurity content and grain size increase along with the age of snow, decreasing the surface reflectance. This evolution is also influenced by atmospheric forcings, which are slightly different from one ensemble member to another, enlarging the spread of the ensemble. We can

TCD
9, 6829–6870, 2015

therefore expect that the timing of the available reflectances will strongly affect the impact of their assimilation on the snowpack ensemble simulations.

3.6 Dispersion of the ensemble of Crocus simulations

Here we assess whether our ensemble of simulation represents a realistic spread of SD over time with respect to previous evaluations of the model through a spread-skill plot.

Given that no SD measurements were systematically carried out at the CdL site, we were not able to evaluate our ensemble spread from SAFRAN-Crocus simulations with a time series of in situ measurements at this site. But, as demonstrated by Fortin et al. (2014), the ability of the ensemble spread to depict the simulation error can be evaluated by the comparison of the root-mean-squared error (RMSE) and the ensemble spread (Spd) with respect to the ensemble mean. The two terms are defined as follows, for a variable X,

$$\mathrm{RMSE}(X) = \left(\frac{1}{M} \sum_{n=1}^{M} \left(X_n - X^{\mathrm{truth}} \right)^2 \right)^{1/2}, \tag{3}$$

$$\mathrm{Spd}(X) = \left(\frac{1}{M} \sum_{k=1}^{M} \frac{1}{N_\mathrm{e}} \sum_{n=1}^{N_\mathrm{e}} \left(X_{k,n} - \overline{X_k} \right)^2 \right)^{1/2}, \tag{4}$$

where M represents the number of time steps and N_e the size of the ensemble. The value from SAFRAN-Crocus simulation is given by X_n, and X^{truth} is the value from the reference. The value of the ensemble member n at the date k is $X_{k,n}$ and $\overline{X_k}$ is the mean of the ensemble at the date k. RMSE and Spd are computed at observation times.

Consequently, we compare the Spd of our ensemble simulation at the CdL site with a SAFRAN-Crocus RMSE over a larger domain. In that purpose, we used roughly 60

TCD
9, 6829–6870, 2015

daily snow depth measurements stations from the Météo-France observation stations network. Each of these stations are within the same altitude range than the CdL site (1800–2200 m a.s.l.). The results are reported in Fig. 2.

Figure 2 shows that, over the 2010/11 season, the SAFRAN-Crocus RMSE is roughly two times higher than the SD dispersion (Spd) of our ensemble. This means that our ensemble is under-dispersive in terms of SD. This may be explained, in part, by the fact that the perturbations calibration is based on statistics for only one location (CdP) which is not highly affected by wind erosion/accumulation in contrast to many of the others measurements sites. In addition, only meteorological errors are considered in our ensemble whereas the model error likely also contribute to the simulation error.

Nonetheless, given that experiments in the present work are twin and that the observations are selected within the ensemble, the impact of this under dispersion is not crucial for our study but must be considered while using real data.

4 Data assimilation setup

This section describes the assimilation framework and the assimilation strategies designed for this study prior presenting results of assimilation experiments (Sects. 5 and 6). First of all, the experimental setup and diagnostics applied in this study are detailed before describing the two observations datasets used for assimilation. An overview of the SIR filter is given at the end of this section and more physics details are provided in the Appendix A.

4.1 General settings and diagnostics

The assimilation experiments are twin, meaning that the observations are synthetic and come from an independent model simulation. They are performed over five winter seasons at the CdL area.

TCD
9, 6829–6870, 2015

A control simulation is first obtained running Crocus forced by one perturbed meteorological forcing, as detailed in Sect. 3.3. The virtual observations used in all the assimilation experiments reported in Sects. 5 and 6 are extracted from this control simulation. The control simulation is also considered as the truth to evaluate the performance of data assimilation.

Data assimilation performances are quantified with the ensemble Root Mean Square Error (RMSE), with respect to the truth and by the representation of the 33, 50 and 67 quantiles of the ensemble members on the figures.

For a variable X, the ensemble RMSE is defined as:

$$\mathrm{RMSE}(X) = \left(\frac{1}{N_\mathrm{e}} \sum_{n=1}^{N_\mathrm{e}} \left(X_n - X^\mathrm{truth} \right)^2 \right)^{1/2}, \quad (5)$$

where N_e represents the size of the ensemble, X_n the value from the ensemble member n, and X^truth the value from the control simulation. RMSE are computed at observation times. The uncertainty on the melt-out date is quantified as the difference (in days) between the first and the latest full melted member.

4.2 Nature of the assimilated observations

The first set of observations is composed of surface reflectances of the first seven bands of MODIS (central wavelengths: 460, 560, 640, 860, 1240, 1640, 2120 nm; Hall and Riggs, 2007). Snow surface reflectances in the visible and near-infrared spectra are sensitive to the properties of the first millimeters to the first centimeters of the snowpack for a given wavelength (Li et al., 2001). They are mainly varying with snow microstructure (near-infrared part) and impurity content (visible part) (Warren, 1982). The reflectance observations error variances, necessary for the assimilation, are defined according to Wright et al. (2014). They are prescribed to 7.1×10^{-4}, 4.6×10^{-4}, 5.6×10^{-4}, 5.6×10^{-4}, 2.0×10^{-3}, 1.5×10^{-3} and 7.8×10^{-4}, for the seven

TCD
9, 6829–6870, 2015

bands, respectively. In the framework of our twin experiments, the covariance matrix of observation errors is diagonal.

Note that the TARTES model calculates bi-hemispherical reflectances while the satellite measurements provides directly hemispherical-conical top of atmosphere reflectances (Dumont et al., 2012). This difference should be considered when the true MODIS data will be assimilated. In the later case, atmospheric and directional corrections of the reflectances must be performed, adding uncertainties to the simulation system.

The second set of observations is composed of snow depth (SD) observations. Previous studies have indeed reported that the assimilation of snowpack bulk variables such as SD greatly improve snow estimations (Morin, 2014; Liu et al., 2013). However, SD observations are only available at one point. In our study, the observation error variance of SD is taken to 0.003 m (corresponding to a standard deviation of about 5 cm). The impact of SD assimilation is detailed in Sect. 6.3.

The setup designed in our study (one point, twin experiments) allows relevant comparisons of the benefits of assimilating separately or jointly the two above mentioned types of observations.

4.3 Assimilation method: the particle filter

The data assimilation method has been chosen after considering the requirements and the possible degrees of freedom that our problem imposes or offers.

Firstly, we require that the method quantifies uncertainties. This plays in favor of ensemble methods (e.g. Blayo et al., 2014). Secondly, we prefer an already existing and well tested method. This argues for the Ensemble Kalman Filter (EnKF, Evensen, 2009) or the particle filter (Van Leeuwen, 2009, 2014). Thirdly, the method should not rely on assumptions about the physical system, such as linearity or weak nonlinearity, because the physics of our model are nonlinear. This draws us toward the particle filter. Fourthly, the method should be easy to implement for this first study. Abaza et al. (2015) assessed the effectiveness assimilating streamflow data using an EnKF sequential

TCD
9, 6829–6870, 2015

procedure but implemented in a simplest snow scheme than Crocus. The fact that the EnKF involves state-averaging operations, to which Crocus hardly complies due to its varying number of snowpack layers, argues in favor of the particle filter. Note that Dechant and Moradkhani (2011) also chose the SIR filter for the assimilation of microwave radiances in a snowpack model. The major drawback of the particle filter is that it is not applicable to high-dimensional systems (Snyder et al., 2008) because it quickly degenerates (all ensemble members converge toward a unique and spurious model trajectory). But our model, with hardly more than a few hundreds of variables, is not high-dimensional. Our experiments show it indeed does not degenerate if a well-tested resampling method is used, with ensembles of a few hundreds of members only. Thus, we choose the *Sequential Importance Resampling* (SIR) filter (Gordon et al., 1993), which is a particular flavor of the particle filter. Our ensembles are composed of 300 members.

The SIR filter seeks to represent the probability density function (pdf) of the model state by a discrete set (an ensemble) of states commonly called particles. The propagation over time of all particles, through the nonlinear model equations, describes the evolution of the model pdf. When observations are available, the ensemble is updated following two steps: (i) the particles are weighted according to their respective distances to the observations, and (ii) the pdf defined by the newly weighted particles is resampled by ruling out particles with negligible weights, and duplicating particles with large weights, so that the updated pdf is again represented by an ensemble of equally-weighted particles. The new ensemble is then ready to be propagated in time by the model. As long as a particle is not removed, it keeps its original perturbed forcing to be propagated. Inversely, a new perturbed forcing is attributed to a duplicated particle to the propagation up to the next analysis. The governing equations of the data assimilation scheme are given in the Appendix A and more details are presented in Van Leeuwen (2009) or Van Leeuwen (2014).

TCD
9, 6829–6870, 2015

5 Assimilation of MODIS-like reflectances

In this section, we assess to what extent the assimilation of the available MODIS-like reflectance observations allows the accurate estimation of snowpack properties throughout the season. This experiment will be considered as our baseline experiment.

Data assimilation results for the 640 and 1240 nm reflectance (first and fifth MODIS bands) and for SD and SWE over the hydrological season 2010/11 are shown in Fig. 3. To mimic real cloud conditions, reflectances are assimilated at 34 clear sky days of the season. We define a clear sky date according the real MODIS data as the complete absence of cloud for the pixel covering the satellite measurement site. The corresponding 640 and 1240 nm reflectance observations are shown by the red dots in Fig 3a and b. The control simulation (from which the observations are drawn) is shown by the red lines.

All along the season, the envelops of SD and SWE ensembles (Fig 3, blue envelops) include the control simulation, which is a prerequisite for the good behaviour of the assimilation. Overall, the assimilation of reflectance observations reduces the uncertainties in the estimation of the snowpack characteristics throughout the season. This is observed in Fig. 3, where the blue envelops are narrower than the grey ones (ensemble without assimilation, reported from Fig. 1). In particular, the snow melt-out date is estimated much more accurately with the assimilation of reflectances: the uncertainty drops from 24 days without assimilation to 9 days with assimilation.

Figure 4 shows the time evolution of the RMSE with assimilation just before and just after the filter analysis (blue solid and blue dotted lines, respectively) compared to the RMSE without assimilation (grey lines). The RMSE of the ensemble with assimilation is always lower than the RMSE without assimilation by a factor of 1.9 on a seasonal average (Table 2: seasonal RMSE SD: 0.07 m; SWE: 19.7 $kg\,m^{-2}$ compared to 0.13 m and 35.4 $kg\,m^{-2}$ from the ensemble without assimilation). It is remarkable that, despite this significant improvement, there is most of the time no strong reduction of the RMSE after a single analysis. The reduced RMSEs with assimilation are consequently due to

TCD
9, 6829–6870, 2015

the continuous flow of observations through the season, highlighting the role of model dynamics.

The strongest impacts of the assimilation of reflectances occur right after extended and unobserved periods without precipitation. During these periods (e.g. from 7 to 14 December 2010, or from 11 to 21 January 2011), the ensemble uncertainties on reflectances, SD and SWE grow under the influence of the perturbed forcings including the perturbed impurity deposition rate. Observations of reflectances have a large impact when they are used. However, since reflectance observations are poorly sensitive to the inner snowpack hidden by recent snowfalls, the uncertainties on SD and SWE accumulated earlier and not corrected by past analysis remain, which ultimately results in limited corrections on SD and SWE (for example, on 28 January 2011), and sustained ensemble spreads and RMSE throughout the season.

After a significant snowfall, the uncertainties in SD and SWE may increase, and the assimilation of reflectances generally has a very small impact on these two variables. Indeed, the uncertainty in the amount of snowfall (translated here in perturbations on the snowfall rate) tends to increase the ensemble spread and RMSE on SD and SWE. On top of this, whether it be in the visible range of wavelengths sensitive to the impurity content or in the infrared part where changes on the microstructure dominates, a snowfall resets the whole ensemble to a unique set of reflectance values. This makes the discrimination between members impossible only from the reflectances, and the analysis provides a rather small uncertainty reduction for SD and SWE. This is illustrated on the 10 November and the 1 December 2010, for example.

The remarks stated above for the season 2010/11 hold for the other seasons. Figure 5 reports the time evolution of the SD and SWE RMSEs for all the selected seasons, in the experiments without assimilation (red lines) and with assimilation of reflectances (blue line; the experiments shown in green and black are discussed in the next section). The SD and SWE RMSEs coarsely decrease twofold on average with assimilation. The error reduction is particularly marked at the end of the seasons.

TCD
9, 6829–6870, 2015

Consequently, our ability to control the seasonal evolution of the snowpack with the assimilation of reflectances is demonstrated, though it meets limitations. In particular, the reduction of the snowpack SD and SWE ensemble spread greatly depends on the timing of the assimilated observations.

6 Sensitivity to the nature and the timing of observations

6.1 Impact of clouds coverage on the experiment

The presence of clouds strongly reduces the number of optical data available for assimilation. To investigate the impact of the limited number of available data, an experiment similar to the first one (see Sect. 5) is carried out but assimilating an observation every day, (134 days) instead of 34 days in the baseline experiment. Figure S2 in the Supplement presents the results with the blue patterns representing the envelops of the ensemble assimilating daily MODIS-like observations and the grey patterns the envelops of the baseline experiment, reported from Fig. 3.

Obviously, in this second experiment, the spread of the 640 nm reflectance ensemble is greatly reduced (Fig. S2a). The ensemble members perfectly fit the reflectance observations and do not show any extended periods with a large range of reflectance values anymore. Compared to the baseline experiment (grey envelops), the uncertainties in the snow melt-out date is also reduced to 3 days. However during the major part of the winter, the SD and SWE ensemble spreads (Fig. S2b and c: blue envelops) are comparable to the spreads obtained in the baseline experiment (Fig. S2b and c: grey envelops). This is also reflected in Table 2: The seasonal RMSEs on SD and SWE are 0.05 m and 14.4 $kg\,m^{-2}$, respectively, against 0.07 m and 19.7 $kg\,m^{-2}$ in the baseline experiment. This shows that the limited number of satellite data due to realistic cloud conditions are not necessarily harmful to the estimation of the snowpack state. Note that this conclusion holds here for bulk variables such as SD and SWE. The

TCD
9, 6829–6870, 2015

estimation of other physical properties of the snowpack will be addressed in a future work using real observations.

6.2 On the timing of observations

The baseline experiment suggests that the timing of observations may largely determine the quality of the assimilation process. To explore the role of the timing, four additional assimilation tests are designed for which MODIS-like reflectances are assimilated (i) only at the beginning of the season (before 31 December 2010, Fig. S3), (ii) only in the second part of the snow season (after 31 December 2010, Fig. S4), (iii) only after several day-long periods without precipitations (Fig. S5) and (iv) only right after snowfalls (Fig. S6).

In case (i), results show that even if the SD and SWE spreads are reduced during the assimilation period, the assimilation has almost no effect on the snow estimates during the snow melt. The ensemble spread retrieves to almost the same value than the experiment without assimilation. The uncertainty of the snow melt-out date is reduced to 22 days only, in comparison with 24 days without assimilation. As for case (ii), the spread reduction becomes quite discernible roughly 2 months after the first assimilation date and never reaches the value of the baseline experiment. The uncertainty of the snow melt-out date is however reduced to 11 days. This demonstrates that it is essential to assimilate reflectances over the entire season to compensate the fast growth of the snowpack ensemble in response to the uncertainties in the meteorological forcing.

In both cases (iii) and (iv), reflectances are assimilated at only 7 dates of the season. Case (iii) exhibits a larger SD and SWE spreads reduction compared to case (iv). The uncertainty on the snow melt-out date drops to 9 days in case (iii) while it stays to 23 days in case (iv). In absence of precipitation, the snow surface is aging, leading to a decrease of reflectance values and a spread of the reflectance ensemble (Fig. S5a). Therefore, an observation after such a period provides a significant amount of information and produces an efficient analysis. On the contrary, solid precipitation resets the reflectance to high values and limits the spread of the reflectance ensemble

TCD
9, 6829–6870, 2015

(Fig. S6a) leading to a limited efficiency of the ensemble analysis. Assimilating only a few observations well distributed in time nearly leads to the same uncertainty of SD and SWE estimates as the baseline experiment assimilating 34 observations (Table 2: seasonal RMSE SD: 0.07 m; SWE: 21.8 kg m^{-2} compared to baseline experiment 0.07 m and 19.7 kg m^{-2}, respectively).

Consequently, the time distribution of the observation turns out to be a key element in the expected success of the assimilation of reflectance observations. The end of an extended period without precipitation, when the surface snow layer is aging, is the best time to assimilate reflectances.

6.3 Assimilation of snow depths

To better evaluate the impact of the reflectance assimilation, we here compare the baseline experiment to an experiment assimilating synthetic SD observations keeping the same time distribution of the observations. Apart from the different nature of the observations, the assimilation setup is the same as the one described in Sect. 5 including the time frequency of observations. The results are displayed in Fig S7.

The assimilation of SD greatly improves the estimates of SD and SWE (Fig. S7b and c). The spread reduction is much stronger than with the assimilation of reflectance observations (Table 2: the seasonal RMSE on SD and SWE are 0.03 m and 7.4 kg m^{-2}, respectively, against 0.07 m and 19.7 kg m^{-2} in the baseline experiment) and is maintained all along the season. Figure 5 also shows that this is the case for the 5 studied seasons. The uncertainty on the snow melt-out date is decreased to 8 days compared to 9 assimilating MODIS-like reflectances and 24 days without assimilation for the 2010/11 season. Note that the spread reduction of the reflectance ensemble is very limited compared to the baseline experiment. This is consistent with the fact that while SD and SWE are better estimated in the case of SD simulation, the surface and inner physical properties of the snowpack are less impacted than in the case of assimilating reflectance observations.

TCD
9, 6829–6870, 2015

Figure S7 shows that, at the beginning of the snow season (before 16 November 2010) and for a thin snowpack (less than 20 cm), SD assimilation seems to have less impact than reflectance assimilation. Indeed, with a thin snowpack, visible wavelengths penetrate down to the ground, and reflectance contains information on the whole snowpack. In this case, reflectance contains more information than SD. This could explain the better performance of the baseline experiment.

An additional experiment (not shown here) was also conducted assimilating daily synthetic SD observations because such measurements are usually daily available at about 60 different stations in the French Alps. This shows that on the contrary to reflectance assimilation, for SD assimilation, the more frequent the observations, the greater the spread reduction (seasonal RMSE SD: 0.02 m; SWE: 4.7 $kg\,m^{-2}$).

Excepted for thin snow cover, the assimilation of SD observations outperforms reflectance assimilation in terms of SWE and SD estimates and seems to be less affected by the time distribution of the observations. However, this experiment assimilating a bulk variable highlights the good performance of the assimilation using reflectance observations (a "surface" information only) to correct the whole snowpack estimation.

6.4 Combining reflectance and snow depth assimilation

Though the assimilation of SD observations generally outperforms reflectance assimilation, spatialized SD measurements are rarely available over large areas on a daily basis. In-situ SD observations give information only at the measurement point and many studies attest to the strong spatial variability of the snow cover (e.g. López-Moreno et al., 2011; Veitinger et al., 2014; Bühler et al., 2015). Airborne LiDAR or ground based laser LiDAR provide accurate SD measurements with fine resolution, but their punctual usage in time limits their utility for operational applications. So, one can imagine that over a mountain range, SD measurements are available at several locations for only a few dates in the season (e.g. occasional snow course, crowd-sourcing, ski resorts observations). This scenario motivates the set-up of the

TCD
9, 6829–6870, 2015

following experiment. The experimental setup is the same as the baseline reflectance assimilation scheme previously described with an extra SD observation the 10th of each month. Results are compared to the previous experiments in Fig. 5.

Combining the assimilation of MODIS-like reflectances with the assimilation of synthetic SD observations provides a benefit compared to assimilating reflectance only (Fig. 5, black and blue lines respectively). (i) In presence of a thin snow cover, the SD and SWE RMSEs of the combined reflectances and SD ensembles are reduced as the ones from the assimilation of the reflectance only. (ii) Almost all along the season, SD and SWE RMSEs remain below the reflectance assimilation RMSE thanks to SD assimilation. The combined assimilation leads to SWE seasonal RMSE of 9.6 $\mathrm{kg\,m^{-2}}$ to be compared to 7.4 $\mathrm{kg\,m^{-2}}$ for the experiment assimilating SD observations and 19.7 $\mathrm{kg\,m^{-2}}$ for the baseline reflectances assimilation experiment (Table 2).

These results encourage to combine these two datasets in operational applications. However, given the strong spatial variability of the snow cover, the spatial representativity of SD measurements may make their assimilation questionable. This issue should be addressed with experiments over two-dimensional, realistic domains.

7 Conclusions

This study investigates the assimilation of MODIS-like reflectances from visible to near-infrared (the first seven bands) into the multilayer snowpack model Crocus. The direct use of reflectance data instead of higher level snow products limits uncertainties due to retrieval algorithms. For the assimilation, we implement a particle filter. A particle filter is chosen because (i) it is an ensemble method providing estimate uncertainties, and (ii) it is easily implemented (in comparison with other assimilation methods) with Crocus model, characterized by strong nonlinearities and its lagrangian representation of the snowpack layering. Given that the major source of error in snowpack simulations can be attributed to meteorological forcings, a stochastic perturbation method is designed to generate an ensemble of possible meteorological variables. This algorithm uses

TCD
9, 6829–6870, 2015

a First Order Auto Regressive model to account for the temporal correlations in the meteorological forcing uncertainties. This ensemble of meteorological forcings is then applied to generate the ensemble of snowpack simulations for the assimilation. Twin experiments were conducted at one point in the French Alps, the Col du Lautaret, over five hydrological years. The assimilated reflectance data corresponds to the first seven spectral bands of the MODIS sensors.

Reflectance assimilation using only data from clear-sky days improves the SD and SWE seasonal RMSE by a factor close to 2. The uncertainty on the snow melt-out date drops to 9 days compared to 24 without assimilation. Additional assimilation tests using different time distributions of the observations show that (i) reflectance assimilation greatly improves snowpack estimates if the observation comes after an extended period without precipitation, (ii) the assimilation has almost no impact if it comes right after a snowfall, and (iii) using only a few observations with the appropriate timing, i.e. after extended periods without precipitation, provides results almost as good as assimilating reflectances on a daily basis.

The assimilation of synthetic SD observations leads to a decrease of SD and SWE RMSE by a factor of more than 4. The uncertainty on the snow melt-out date is reduced to 8 days. The assimilation of SD observations generally outperforms reflectance assimilation except for thin snowpacks, typically less than 20 cm. However, whereas optical reflectance maps can be obtained daily thanks to spaceborne sensors such MODIS or VIIRS, SD measurements are rarely available either over large areas or at the same time frequency. Combining reflectance assimilation with only 4 SD observations assimilation during the snow season leads to a decrease of SD and SWE RMSE by a factor close to 3.

This study provides a general theoretical framework to test the efficiency of several kind of data assimilation in a snowpack model and highlights the benefit of using remotely sensed optical surface reflectance in the assimilation scheme to provide significant improvements of the snowpack SD and SWE estimates. Even if the assimilation of SD outperforms the assimilation using reflectance data, the sparsity of

TCD
9, 6829–6870, 2015

in situ measurements in space and/or time strongly reduces their utility in real data assimilation systems. Nevertheless, given their complementary features, combining remotely sensed reflectances and SD data, when available, would definitely improve snowpack simulations.

This study presents a first attempt to assimilate snow observations into the Crocus snowpack model with the overarching objective of improving operational snowpack forecasting. The next steps to proceed toward operational applications must include the assimilation of actual satellite data and the spatialization of the assimilation on larger domains. These steps include several challenges such as the increased calculation costs and degrees of freedom, and the need for a physically consistent 2-D meteorological ensemble, what will be addressed in future work.

Appendix A: Particle filter and sequential importance resampling, definitions

In a discrete-time space model, the state of a system evolves according to:

$$\boldsymbol{x}_k = f_k(\boldsymbol{x}_{k-1}, \boldsymbol{v}_{k-1}),$$

where $\boldsymbol{x}_k$ is the state vector of the system at time k, $\boldsymbol{v}_{k-1}$ is the state noise vector and f_k is the non-linear and time-dependent function describing the evolution of the state vector.

Information about $\boldsymbol{x}_k$ is obtained though noisy measurements, y_k, which are governed by the observation operator equation:

$$y_k = h_k(\boldsymbol{x}_k, \boldsymbol{n}_k), \tag{A1}$$

where h_k is a possibly non-linear and time-dependent function linking the state vector to the observation (observation operator) and $\boldsymbol{n}_k$ is the measurement noise vector.

The filtering problem is to estimate sequentially the values of $\boldsymbol{x}_k$, given the observed values $y_0, \ldots, y_k$, at any time step k. In a Bayesian setting, this problem can be

TCD
9, 6829–6870, 2015

formalized as the computation of the distribution $p(\boldsymbol{x}_k|y_{1:k})$, which can be done recursively in two steps:

Prediction step:

$$p(\boldsymbol{x}_k|y_{1:k-1}) = \int p(\boldsymbol{x}_k - 1|y_{k-1})p(\boldsymbol{x}_k|\boldsymbol{x}_{k-1})\mathrm{d}\boldsymbol{x}_{k-1}. \quad \text{(A2)}$$

Updating step to estimate $p(\boldsymbol{x}_k|y_{1:k})$ using Bayes'rule:

$$p(\boldsymbol{x}_k|y_{1:k}) \propto p(y_k|\boldsymbol{x}_k)p(\boldsymbol{x}_k|y_{1:k-1}). \quad \text{(A3)}$$

In the particle filter, the prior pdf is represented by equally-weighted delta functions centered on the ensemble members or particles:

$$p(\boldsymbol{x}_{k-1}|y_{1:k-1}) = \frac{1}{N}\sum_{i=1}^{N}\delta\left(\boldsymbol{x}_{k-1} - \boldsymbol{x}_{k-1}^{i}\right),$$

where N is the ensemble size. With this representation, the propagation step A2 provides:

$$p(\boldsymbol{x}_k|y_{1:k-1}) = \frac{1}{N}\sum_{i=1}^{N}\delta\left(\boldsymbol{x}_k - \boldsymbol{x}_k^{i}\right),$$

where $\boldsymbol{x}_k^i = f\left(\boldsymbol{x}_{k-1}^i, \boldsymbol{v}_{k-1}^i\right)$; $\boldsymbol{v}_{k-1}^i$ is a realization of the noise $\boldsymbol{v}_{k-1}$. Then the analysis step follows with:

$$p(\boldsymbol{x}_k|y_{1:k}) = \sum_{i=1}^{N} w_k^i \delta\left(\boldsymbol{x}_k - \boldsymbol{x}_k^i\right),$$

where the w_k^i are the particle weights, normalized to sum up to 1, and given by:

$$w_k^i \propto p\left(y_k|\boldsymbol{x}_k^i\right).$$

TCD
9, 6829–6870, 2015

To compute the weights, the error n_k of the observation operator h_k (Eq. A1) is often considered additive and Gaussian with mean 0 and covariance matrix R_k, so that the likelihood $p\left(y_k|\boldsymbol{x}_k^i\right)$ writes:

$$p\left(y_k|\boldsymbol{x}_k^i\right) \propto \exp\left(-\frac{1}{2}\left(y_k - h\left(\boldsymbol{x}_k^i\right)\right)^T R^{-1}\left(y_k - h\left(\boldsymbol{x}_k^i\right)\right)\right).$$

After the computation of the weights, the ensemble is resampled: particles with zero or negligible weights are ruled out; particles with large weights are duplicated a number of times commensurate with their weights. Several algorithms exist for this resampling step; we use the one of Kitagawa.

The Supplement related to this article is available online at doi:10.5194/tcd-9-6829-2015-supplement.

Acknowledgements. We gratefully acknowledge funding from Labex OSUG@2020 (Investissements d'avenir – ANR10 LABX56) and Fondation Eau Neige et Glace. This work has also been supported by the INSU/LEFE/MANU program. The development of the radiative model TARTES has been funded by the French ANR MONISNOW project, number ANR-11-JS56-0005.

References

Abaza, M., Anctil, F., Fortin, V., and Turcotte, R.: Exploration of sequential streamflow assimilation in snow dominated watersheds, Adv. Water Resour., 80, 79–89, doi:10.1016/j.advwatres.2015.03.011, 2015. 6845

Andreadis, K. M. and Lettenmaier, D. P.: Assimilating remotely sensed snow observations into a macroscale hydrology model, Adv. Water Resour., 29, 872–886, doi:10.1016/j.advwatres.2005.08.004, 2006. 6831

Bartelt, P. and Lehning, M.: A physical SNOWPACK model for the Swiss avalanche warning: Part I: Numerical model, Cold Reg. Sci. Technol., 35, 123–145, doi:10.1016/S0165-232X(02)00074-5, 2002. 6831

TCD
9, 6829–6870, 2015

Bavay, M., Grünewald, T., and Lehning, M.: Response of snow cover and runoff to climate change in high Alpine catchments of Eastern Switzerland, Adv. Water Resour., 55, 4–16, doi:10.1016/j.advwatres.2012.12.009, 2013. 6830

Blayo, É., Bocquet, M., Cosme, E., and Cugliandolo, L. F.: Advanced Data Assimilation for Geosciences: Lecture Notes of the Les Houches School of Physics: Special Issue, June 2012, Oxford University Press, Oxford, UK, 2014. 6845

Boone, A. and Etchevers, P.: An intercomparison of three snow schemes of varying complexity coupled to the same land surface model: Local-scale evaluation at an Alpine site, J. Hydrometeorol., 2, 374–394, doi:10.1175/1525-7541(2001)002<0374:AIOTSS>2.0.CO;2, 2001. 6834

Brun, E., Martin, E., Simon, V., Gendre, C., and Coléou, C.: An energy and mass model of snow cover suitable for operational avalanche forecasting, J. Glaciol., 35, 333–342, 1989. 6831, 6833

Brun, E., David, P., Sudul, M., and Brunot, G.: A numerical model to simulate snow-cover stratigraphy for operational avalanche forecasting, J. Glaciol., 38, 13–22, 1992. 6831, 6833, 6835, 6841

Brun, F., Dumont, M., Wagnon, P., Berthier, E., Azam, M. F., Shea, J. M., Sirguey, P., Rabatel, A., and Ramanathan, Al.: Seasonal changes in surface albedo of Himalayan glaciers from MODIS data and links with the annual mass balance, The Cryosphere, 9, 341–355, doi:10.5194/tc-9-341-2015, 2015. 6832

Bühler, Y., Marty, M., Egli, L., Veitinger, J., Jonas, T., Thee, P., and Ginzler, C.: Snow depth mapping in high-alpine catchments using digital photogrammetry, The Cryosphere, 9, 229–243, doi:10.5194/tc-9-229-2015, 2015. 6852

Carpenter, T. M. and Georgakakos, K. P.: Impacts of parametric and radar rainfall uncertainty on the ensemble streamflow simulations of a distributed hydrologic model, J. Hydrol., 298, 202–221, doi:10.1016/j.jhydrol.2004.03.036, 2004. 6831

Castebrunet, H., Eckert, N., Giraud, G., Durand, Y., and Morin, S.: Projected changes of snow conditions and avalanche activity in a warming climate: the French Alps over the 2020–2050 and 2070–2100 periods, The Cryosphere, 8, 1673–1697, doi:10.5194/tc-8-1673-2014, 2014. 6834

Cordisco, E., Prigent, C., and Aires, F.: Snow characterization at a global scale with passive microwave satellite observations, J. Geophys. Res., 111, D19102, doi:10.1029/2005JD006773, 2006. 6832

TCD
9, 6829–6870, 2015

De Lannoy, G. J., Reichle, R. H., Arsenault, K. R., Houser, P. R., Kumar, S., Verhoest, N. E., and Pauwels, V.: Multiscale assimilation of Advanced Microwave Scanning Radiometer–EOS snow water equivalent and Moderate Resolution Imaging Spectroradiometer snow cover fraction observations in northern Colorado, Water Resour. Res., 48, W01522, doi:10.1029/2011WR010588, 2012. 6831

Dechant, C. and Moradkhani, H.: Radiance data assimilation for operational snow and streamflow forecasting, Adv. Water Resour., 34, 351–364, doi:10.1016/j.advwatres.2010.12.009, 2011. 6831, 6846

Deodatis, G. and Shinozuka, M.: Auto-regressive model for nonstationary stochastic processes, J. Eng. Mech.-ASCE, 114, 1995–2012, doi:10.1061/(ASCE)0733-9399(1988)114:11(1995), 1988. 6838

Doherty, S. J., Grenfell, T. C., Forsström, S., Hegg, D. L., Brandt, R. E., and Warren, S. G.: Observed vertical redistribution of black carbon and other insoluble light-absorbing particles in melting snow, J. Geophys. Res.-Atmos., 118, 5553–5569, doi:10.1002/jgrd.50235, 2013. 6836

Domine, F., Sparapani, R., Ianniello, A., and Beine, H. J.: The origin of sea salt in snow on Arctic sea ice and in coastal regions, Atmos. Chem. Phys., 4, 2259–2271, doi:10.5194/acp-4-2259-2004, 2004. 6836

Dong, J., Walker, J. P., Houser, P. R., and Sun, C.: Scanning multichannel microwave radiometer snow water equivalent assimilation, J. Geophys. Res., 112, D07108, doi:10.1029/2006JD007209, 2007. 6831, 6832

Dumont, M., Durand, Y., Arnaud, Y., and Six, D.: Variational assimilation of albedo in a snowpack model and reconstruction of the spatial mass-balance distribution of an alpine glacier, J. Glaciol., 58, 151–164, doi:10.3189/2012JoG11J163, 2012. 6831, 6832, 6845

Dumont, M., Brun, E., Picard, G., Michou, M., Libois, Q., Petit, J., Geyer, M., Morin, S., and Josse, B.: Contribution of light-absorbing impurities in snow to Greenland's darkening since 2009, Nat. Geosci., 7, 509–512, doi:10.1038/ngeo2180, 2014. 6836

Durand, M., Kim, E. J., and Margulis, S. A.: Radiance assimilation shows promise for snowpack characterization, Geophys. Res. Lett., 36, L02503, doi:10.1029/2008GL035214, 2009. 6831, 6838

Durand, Y., Brun, E., Mérindol, L., Guyomarc'h, G., Lesaffre, B., and Martin, E.: A meteorological estimation of relevant parameters for snow models, Ann. Glaciol., 18, 65–71, 1993. 6836, 6837

TCD
9, 6829–6870, 2015

Durand, Y., Giraud, G., Brun, E., Mérindol, L., and Martin, E.: A computer-based system simulating snowpack structures as a tool for regional avalanche forecasting, J. Glaciol., 45, 469–484, 1999. 6830, 6834

Essery, R., Morin, S., Lejeune, Y., and Menard, C. B.: A comparison of 1701 snow models using observations from an alpine site, Adv. Water Resour., 55, 131–148, doi:10.1016/j.advwatres.2012.07.013, 2013. 6831, 6832

Etchevers, P., Golaz, C., and Habets, F.: Simulation of the water budget and the river flows of the Rhone basin from 1981 to 1994, J. Hydrol., 244, 60–85, doi:10.1016/S0022-1694(01)00332-8, 2001. 6834

Evensen, G.: Data Assimilation: the Ensemble Kalman Filter, Springer Science & Business Media, Berlin, 2009. 6845

Fortin, V., Abaza, M., Anctil, F., and Turcotte, R.: Why should ensemble spread match the RMSE of the ensemble mean?, J. Hydrometeorol., 15, 1708–1713, doi:10.1175/JHM-D-14-0008.1, 2014. 6842

Foster, J. L., Sun, C., Walker, J. P., Kelly, R., Chang, A., Dong, J., and Powell, H.: Quantifying the uncertainty in passive microwave snow water equivalent observations, Remote Sens. Environ., 94, 187–203, doi:10.1016/j.rse.2004.09.012, 2005. 6832

Gabbi, J., Huss, M., Bauder, A., Cao, F., and Schwikowski, M.: The impact of Saharan dust and black carbon on albedo and long-term glacier mass balance, The Cryosphere Discuss., 9, 1133–1175, doi:10.5194/tcd-9-1133-2015, 2015. 6836

Gordon, N. J., Salmond, D. J., and Smith, A. F.: Novel approach to nonlinear/non-Gaussian Bayesian state estimation, in: IEE Proc.-F, 140, 107–113, 1993. 6832, 6846

Hall, D. K. and Riggs, G. A.: Accuracy assessment of the MODIS snow products, Hydrol. Process., 21, 1534–1547, doi:10.1002/hyp.6715, 2007. 6844

Jordan, R.: A One-Dimensional Temperature Model for a Snow Cover: Technical Documentation for SNTHERM. 89., Tech. rep., Cold Regions Research and Engineering Lab, Hanover, NH, USA, 1991. 6831

Lehning, M., Völksch, I., Gustafsson, D., Nguyen, T. A., Stähli, M., and Zappa, M.: ALPINE3D: a detailed model of mountain surface processes and its application to snow hydrology, Hydrol. Process., 20, 2111–2128, doi:10.1002/hyp.6204, 2006. 6830

Li, W., Stamnes, K., Chen, B., and Xiong, X.: Snow grain size retrieved from near-infrared radiances at multiple wavelengths, Geophys. Res. Lett., 28, 1699–1702, doi:10.1029/2000GL011641, 2001. 6844

TCD
9, 6829–6870, 2015

Libois, Q., Picard, G., France, J. L., Arnaud, L., Dumont, M., Carmagnola, C. M., and King, M. D.: Influence of grain shape on light penetration in snow, The Cryosphere, 7, 1803–1818, doi:10.5194/tc-7-1803-2013, 2013. 6835

Libois, Q., Picard, G., Dumont, M., Arnaud, L., Sergent, C., Pougatch, E., Sudul, M., and Vial, D.: Experimental determination of the absorption enhancement parameter of snow, J. Glaciol., 60, 714–724, doi:10.1002/2014JD022361, 2014. 6835

Liu, Y., Peters-Lidard, C. D., Kumar, S., Foster, J. L., Shaw, M., Tian, Y., and Fall, G. M.: Assimilating satellite-based snow depth and snow cover products for improving snow predictions in Alaska, Adv. Water Resour., 54, 208–227, doi:10.1016/j.advwatres.2013.02.005, 2013. 6831, 6845

López-Moreno, J. I., Fassnacht, S. R., Beguería, S., and Latron, J. B. P.: Variability of snow depth at the plot scale: implications for mean depth estimation and sampling strategies, The Cryosphere, 5, 617–629, doi:10.5194/tc-5-617-2011, 2011. 6852

Masson, V., Le Moigne, P., Martin, E., Faroux, S., Alias, A., Alkama, R., Belamari, S., Barbu, A., Boone, A., Bouyssel, F., Brousseau, P., Brun, E., Calvet, J.-C., Carrer, D., Decharme, B., Delire, C., Donier, S., Essaouini, K., Gibelin, A.-L., Giordani, H., Habets, F., Jidane, M., Kerdraon, G., Kourzeneva, E., Lafaysse, M., Lafont, S., Lebeaupin Brossier, C., Lemonsu, A., Mahfouf, J.-F., Marguinaud, P., Mokhtari, M., Morin, S., Pigeon, G., Salgado, R., Seity, Y., Taillefer, F., Tanguy, G., Tulet, P., Vincendon, B., Vionnet, V., and Voldoire, A.: The SURFEXv7.2 land and ocean surface platform for coupled or offline simulation of earth surface variables and fluxes, Geosci. Model Dev., 6, 929–960, doi:10.5194/gmd-6-929-2013, 2013. 6834

Morin, S.: Observation and numerical modeling of snow on the ground: use of existing tools and contribution to ongoing developments, Habilitation à diriger des recherches, Université Joseph Fourier, Grenoble, France, 2014. 6845

Morin, S., Lejeune, Y., Lesaffre, B., Panel, J.-M., Poncet, D., David, P., and Sudul, M.: An 18-yr long (1993–2011) snow and meteorological dataset from a mid-altitude mountain site (Col de Porte, France, 1325 m alt.) for driving and evaluating snowpack models, Earth Syst. Sci. Data, 4, 13–21, doi:10.5194/essd-4-13-2012, 2012. 6833, 6838

Noilhan, J. and Planton, S.: A simple parameterization of land surface processes for meteorological models, Mon. Weather Rev., 117, 536–549, doi:10.1175/1520-0493(1989)117<0536:ASPOLS>2.0.CO;2, 1989. 6834

TCD
9, 6829–6870, 2015

Painter, T. H., Barrett, A. P., Landry, C. C., Neff, J. C., Cassidy, M. P., Lawrence, C. R., McBride, K. E., and Farmer, G. L.: Impact of disturbed desert soils on duration of mountain snow cover, Geophys. Res. Lett., 34, L12502, doi:10.1029/2007GL030284, 2007. 6836

Phan, X. V., Ferro-Famil, L., Gay, M., Durand, Y., Dumont, M., Morin, S., Allain, S., D'Urso, G., and Girard, A.: 1D-Var multilayer assimilation of X-band SAR data into a detailed snowpack model, The Cryosphere, 8, 1975–1987, doi:10.5194/tc-8-1975-2014, 2014. 6832

Quintana Segui, P., Moigne, P. L., Durand, Y., Martin, E., Habets, F., Baillon, M., Canella, C., Franchisteguy, L., and Morel, S.: Analysis of near surface atmospheric variables: validation of the SAFRAN analysis over France, J. Appl. Meteorol. Clim., 47, 92–107, doi:10.1175/2007JAMC1636.1, 2008. 6838

Raleigh, M. S., Lundquist, J. D., and Clark, M. P.: Exploring the impact of forcing error characteristics on physically based snow simulations within a global sensitivity analysis framework, Hydrol. Earth Syst. Sci., 19, 3153–3179, doi:10.5194/hess-19-3153-2015, 2015. 6831, 6837

Sirguey, P., Mathieu, R., and Arnaud, Y.: Subpixel monitoring of the seasonal snow cover with MODIS at 250 m spatial resolution in the Southern Alps of New Zealand: methodology and accuracy assessment, Remote Sens. Environ., 113, 160–181, doi:10.1016/j.rse.2008.09.008, 2009. 6832

Snyder, C., Bengtsson, T., Bickel, P., and Anderson, J.: Obstacles to high-dimensional particle filtering, Mon. Weather Rev., 136, 4629–4640, doi:10.1175/2008MWR2529.1, 2008. 6846

Stankov, B. B., Cline, D. W., Weber, B. L., Gasiewski, A. J., and Wick, G.: High-resolution airborne polarimetric microwave imaging of snow cover during the NASA cold land processes experiment, IEEE T. Geosci. Remote, 46, 3672–3693, doi:10.1109/TGRS.2008.2000625, 2008. 6832

Tedesco, M., Reichle, R., Löw, A., Markus, T., and Foster, J. L.: Dynamic approaches for snow depth retrieval from spaceborne microwave brightness temperature, IEEE T. Geosci. Remote, 48, 1955–1967, doi:10.1109/TGRS.2009.2036910, 2010. 6832

Van Leeuwen, P. J.: Particle filtering in geophysical systems, Mon. Weather Rev., 137, 4089–4114, doi:10.1175/2009MWR2835.1, 2009. 6832, 6845, 6846

Van Leeuwen, P. J.: Particle filters for the geosciences, Advanced Data Assimilation for Geosciences: Lecture Notes of the Les Houches School of Physics: Special Issue, June 2012, p. 291, doi:10.1093/acprof:oso/9780198723844.003.0013, 2014. 6832, 6845, 6846

TCD
9, 6829–6870, 2015

Veitinger, J., Sovilla, B., and Purves, R. S.: Influence of snow depth distribution on surface roughness in alpine terrain: a multi-scale approach, The Cryosphere, 8, 547–569, doi:10.5194/tc-8-547-2014, 2014. 6852

Vernay, M., Lafaysse, M., Mérindol, L., Giraud, G., and Morin, S.: Ensemble forecasting of snowpack conditions and avalanche hazard, Cold Reg. Sci. Technol., 120, 251–626, doi:10.1016/j.coldregions.2015.04.010, 2015. 6831

Vionnet, V., Brun, E., Morin, S., Boone, A., Faroux, S., Le Moigne, P., Martin, E., and Willemet, J.-M.: The detailed snowpack scheme Crocus and its implementation in SURFEX v7.2, Geosci. Model Dev., 5, 773–791, doi:10.5194/gmd-5-773-2012, 2012. 6831, 6833, 6835

Warren, S.: Optical properties of snow, Rev. Geophys., 20, 67–89, doi:10.1029/RG020i001p00067, 1982. 6832, 6836, 6844

Warren, S. G. and Clarke, A. D.: Soot in the atmosphere and snow surface of Antarctica, J. Geophys. Res.-Atmos., 95, 1811–1816, doi:10.1029/JD095iD02p01811, 1990. 6836

Wright, P., Bergin, M., Dibb, J., Lefer, B., Domine, F., Carman, T., Carmagnola, C. M., Dumont, M., Courville, Z., Schaaf, C., and Wang, Z.: Comparing MODIS daily snow albedo to spectral albedo field measurements in Central Greenland, Remote Sens. Environ., 140, 118–129, doi:10.1016/j.rse.2013.08.044, 2014. 6844

TCD
9, 6829–6870, 2015

Table 1. Means and standard deviations of the differences between SAFRAN reanalysis and in situ observations (left) and the differences between SAFRAN reanalysis and the ensemble built up in the present study (right), for the perturbed meteorological forcings. The first set of statistics is derived from 18 years of observations and reanalysis at the CdP and the second set is derived from our 300 members ensemble over the 2010/11 hydrological season.

Variables	CdP: Reanalysis – Observations		CdL: Reanalysis – Ensemble	
	Bias	Standard deviations	Bias	Standard deviations
Air temperature (°C)	0.28	1.08	5.0×10^{-3}	1.07
Wind speed ($m\,s^{-1}$)	0.2	1.12	4.0×10^{-4}	0.4
Shortwave radiation ($W\,m^{-2}$)	22.4	79	-3.1×10^{-3}	58.3
Longwave radiation ($W\,m^{-2}$)	−14.0	24.5	2.0×10^{-2}	7.0
Snowfall rate ($kg\,m^{-2}\,h^{-1}$)	-2.0×10^{-2}	0.4	5.0×10^{-3}	0.1
Rainfall rate ($kg\,m^{-2}\,h^{-1}$)	7.2×10^{-3}	0.5	-5.0×10^{-3}	0.1

TCD
9, 6829–6870, 2015

Table 2. Seasonal SD and SWE RMSE computed with respect to the truth for all experiments.

	Fig. 1	Baseline	Fig. S7	Fig. S2	Fig. S3	Fig. S4	Fig. S5	Fig. S6	Fig. 5
SD (m)	0.13	0.07	0.03	0.05	0.05	0.12	0.07	0.12	0.04
SWE ($kg\,m^{-2}$)	35.4	19.7	7.4	14.4	12.9	35.5	21.8	37.2	9.6

TCD
9, 6829–6870, 2015

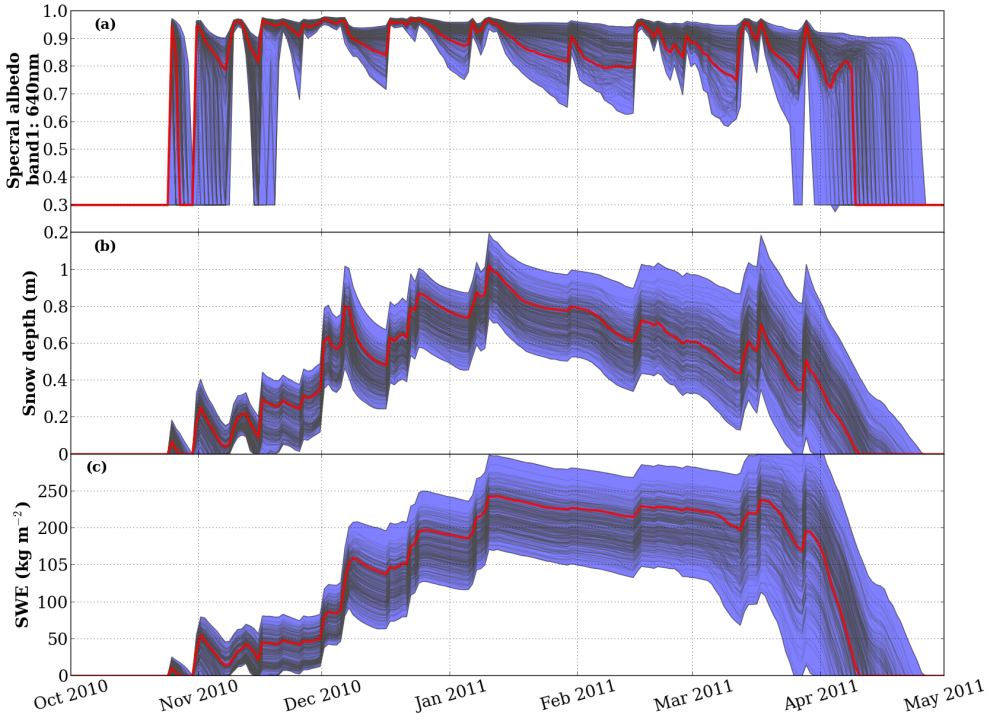

Figure 1. Ensemble simulation with 300 members at the Col du Lautaret site over the 2010/11 hydrological season. **(a)** Reflectance at 640 nm (band 1 of MODIS), **(b)** SD, and **(c)** SWE. On each graph, the red solid line is the simulation forced by the unperturbed SAFRAN analysis. The blue patterns represent the envelops including the 300 members which are shown by the black lines.

TCD
9, 6829–6870, 2015

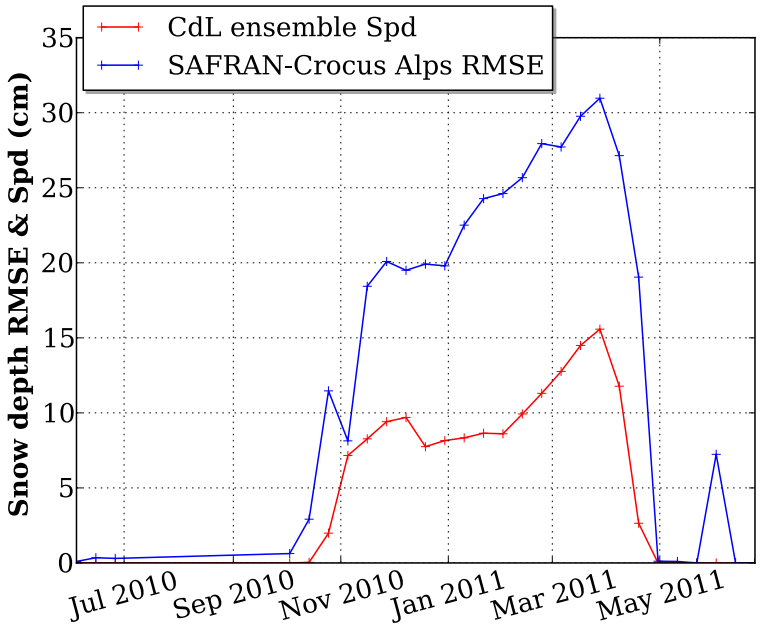

Figure 2. Time evolution over the 2010/11 season of (in red) the SD ensemble Spd with respect to the ensemble mean and (in blue) the SD RMSE between SAFRAN-Crocus estimates and in situ observations.

TCD
9, 6829–6870, 2015

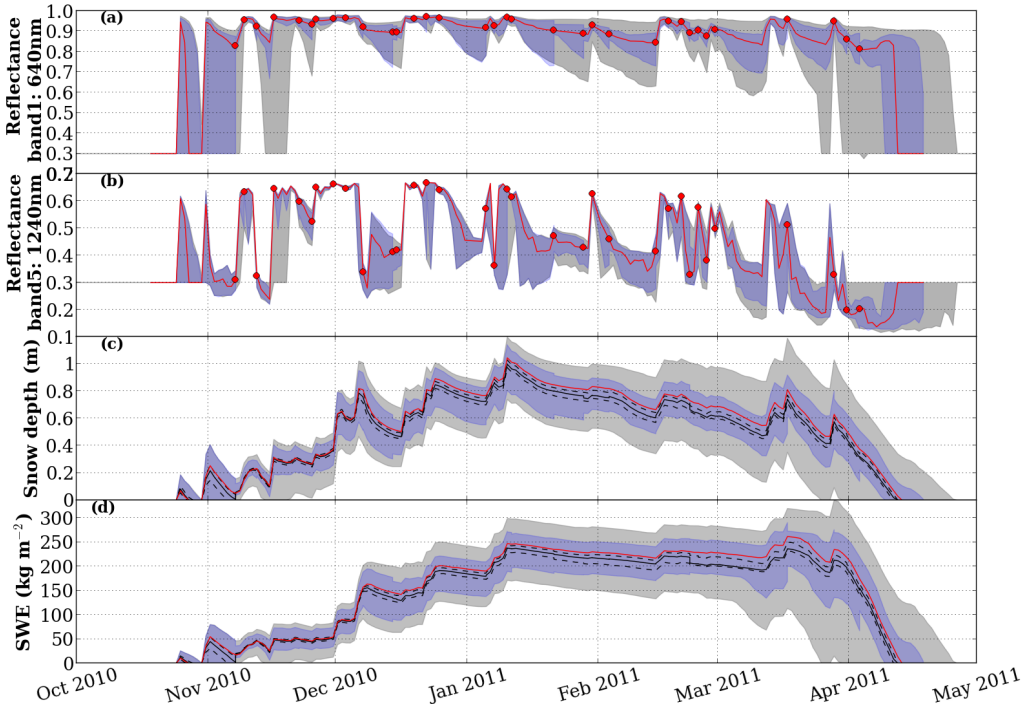

Figure 3. Evolution of the ensemble over the 2010/11 season. **(a)** and **(b)** Reflectance at 640 and 1240 nm (first and fifth MODIS band, respectively), **(c)** SD and **(d)** SWE. The blue patterns represent the envelops of the ensemble assimilating MODIS-like reflectances and the grey patterns the envelops of the ensemble without assimilation. The red lines represent the control simulation (truth). On graph **(a)** and **(b)**, the red dots show the assimilated observations. On both **(c)** and **(d)**, the black solid line shows the 50 % quantiles (median of the ensemble) and the black dotted lines the 33 and 67 % quantiles.

TCD
9, 6829–6870, 2015

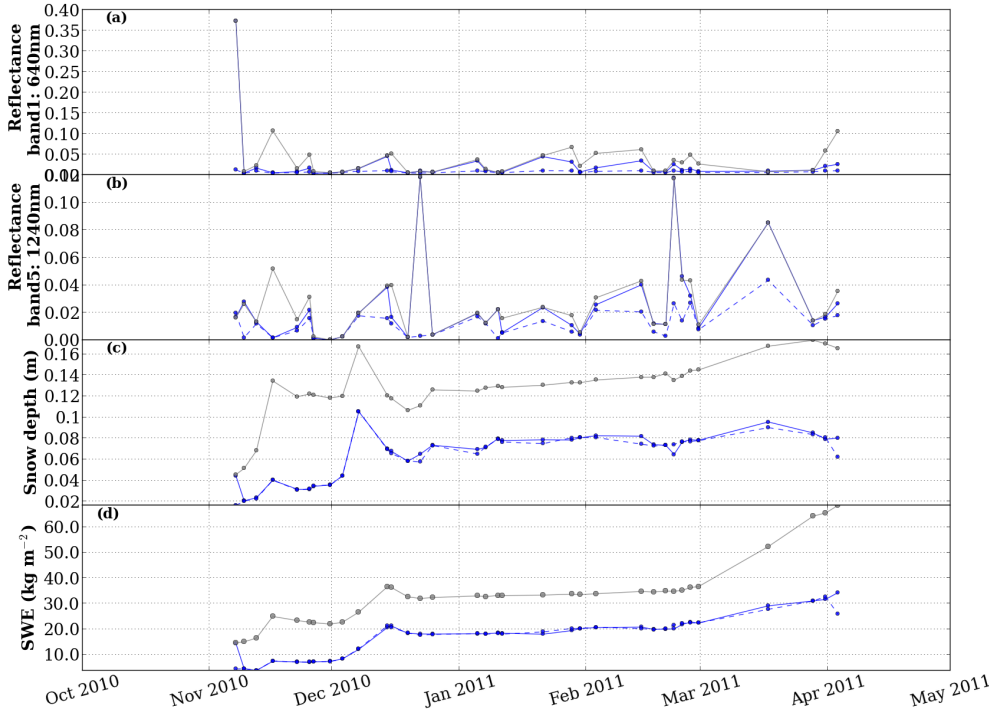

Figure 4. Time evolution of the ensemble RMSEs on **(a)** Reflectance at 640 nm, **(b)** reflectance at 1240 nm, **(c)** SD and **(d)** SWE, over the 2010/11 season, for the run without assimilation (grey lines), and the baseline assimilation experiment (Blue solid line: forecast; blue dotted line: analysis). Dots indicate analysis steps.

TCD
9, 6829–6870, 2015

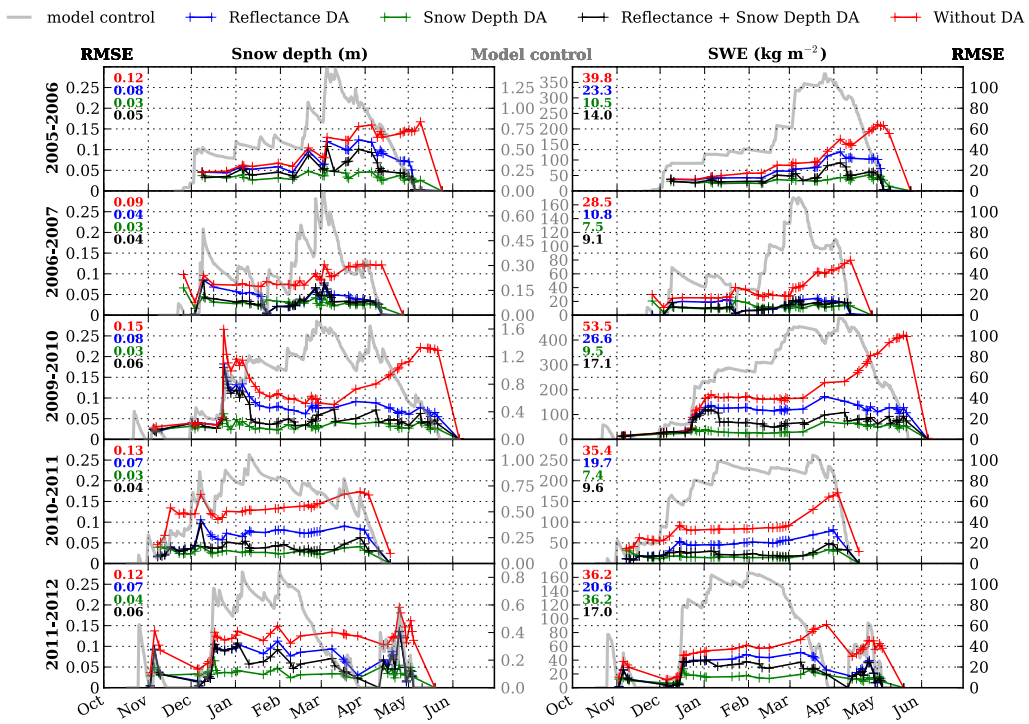

Figure 5. Time evolution of ensemble RMSEs on SD (left) and SWE (right) for the five seasons under study, for the run without assimilation (red lines), the baseline experiment (assimilating reflectances, blue lines), the experiment assimilating SD data (green lines) and the experiment assimilating combined reflectances and SD data (black lines). Crosses indicate analysis steps. Seasonal means are displayed in the upper left corner of each graph. The model control simulation is represented by the grey lines, scaled by the "Model control" *y* axes.

TCD
9, 6829–6870, 2015